The Institute of space and Astronautical Science
Report No. 674, March 1999

Shock Wave Development around Accelerated Bodies at Supersonic Mach Numbers Slightly Larger than One

By

Kunio KUWAHARA and Karl G.ROESNER

(February 2, 1999)

ABSTRACT: Based on Cabannes' [1] analytic investigation on nonstationary attached shock waves around accelerated or decelerated bodies at supersonic velocities, the unsteady supersonic flow around wedge-like and conical bodies is analysed analytically and numerically with respect to the relationship between the curvature of the body contour at the pointed nose and the curvature of attached shock wave at the tip of the body. The body is transformed to rest, and the instantaneous value of the acceleration or deceleration of the flow field is taken into account in the basic equations. In its lowest order of approximation the acceleration or deceleration is linearly combined in a relationship with the curvature of the body shape and the shock at the nose point. By computer algebraic calculations the higher order terms of a series expansion of the relation between the curvatures and the acceleration are determined and compared with numerical simulations on the basis of the Eulerian and the compressible Navier-Stokes-equations.

1. INTRODUCTION

For supersonic flows at Mach numbers close to 1 the behavior of the flow quantities near the attached shock wave are essentially influenced when the flow is accelerated or decelerated. Since Cabannes' investigations [2], [3] on nonstationary attached shock waves, a great interest was shown for the experimental and numerical analysis of nonstationary shock wave problems. Whitham's paper [4] on the flow pattern of a supersonic projectile and Rao's [5] analysis of supersonic bangs, mark the origin of the research concerning the flow near the pointed nose of conical bodies in nonstationary flows.

In the present paper a numerical analysis is performed for the determination of the shock curvature on the basis of a time-dependent calculation of the flow field around accelerated or decelerated bodies of revolution or around wedges. A TVD-scheme is used with an explicit discretization with respect to time. The Riemann solver according to Harten, Lax, and van Leer is applied. The calculations are performed on a Fujitsu machine VPP 300/6 of the Darmstadt Computing Center of the Darmstadt University of Technology [6,7]. A comparison with the known

data from Cabannes' asymptotic analysis is given which shows some differences between the numerical results and the analytical formula which leads to a linear relationship between the curvature of the shock, the curvature of the body shape at the nose κ_{body} and the acceleration of the body:

$$\kappa_{shock}(t) = f(\theta, M, \gamma)\,\kappa_{body} + g(\theta, M, \gamma)\,\frac{a(t)}{c^2} \tag{1}$$

$\kappa_{shock}(t)$ means the instantaneous curvature of the shock wave, f and g are functions of the angle of the velocity with respect to the symmetry line of the flow field, M is the Mach number, γ is the ratio of the specific heat at constant pressure and constant volume, respectively, the acceleration is denoted by a(t), and c is the speed of sound.

2. BASIC EQUATIONS

The time-dependent motion of wedge-like or conical bodies at supersonic velocities in a gas at rest is described relative to a coordinate system which is moving with the body. Therefore, in the case of an accelerated body, the upstream velocity has the negative sign of the instantaneous velocity of the body. In additon, the equation of conservation of momentum is enlarged on the right hand side by an additional force term. The Eulerian equations are used in the following form:

$$\frac{D\bar{v}}{Dt} = -\frac{1}{\rho}\nabla p - \bar{a}\,, \tag{2}$$

while the Navier-Stokes equations are written in the form:

$$\frac{D\bar{v}}{Dt} = -\frac{1}{\rho}\nabla p - \bar{a} + \mu\Delta\bar{v}\,, \tag{3}$$

where ρ is the density, $\vec{v}$ the velocity, and p the pressure and μ the dynamic viscosity of the gas. The operator $\frac{D}{Dt}$ denotes the differentiation along path lines in the flow field, and $\vec{a}$ is the acceleration of the moving body. Also in the energy equation an additional term in added on the right hand side which results in the following from of the equation of consevation of energy for the Eulerian equations:

$$\frac{D}{Dt}\left(e + \frac{1}{2}\bar{v}^2\right) = -\frac{1}{\rho}\nabla(p\bar{v}) - \bar{a}\cdot\bar{v}. \tag{4}$$

e is the specific internal energy of the gas. In the same way the energy equation for an viscous gas is enlarged by the acceleration term on the right hand side. The continuity equation is used in the form:

$$\frac{D\rho}{Dt} + \rho\nabla\cdot\bar{v} = 0\,. \tag{5}$$

As initial condition for the numerical simulations, the calculations are started from a supersonic flow at constant Mach number far upstream. The specific internal energy at infinity is calculated according to the formula:

$$e_\infty = \frac{1}{\gamma(\gamma-1)}\,\frac{\bar{v}^2 f_0}{M_{0\infty}^2}\,. \tag{6}$$

$\vec{v}_{f0}$ and $M_{0\infty}$ are the upstream velocity and the Mach number of the oncoming gas flow. The

boundary conditions are fulfilled according to Fig. 1. The distribution of the flow variables at the inlet $\partial\Omega 1$ are given by the following formulas:

$$\begin{aligned} \rho(t)|_{\partial\Omega_1} &= \rho_\infty, \\ \rho(t)\vec{v}(t)|_{\partial\Omega_1} &= -\rho_\infty \vec{v}_f(t), \\ E(t)|_{\partial\Omega_1} &= \rho_\infty e_\infty + \frac{1}{2}\rho_\infty \vec{v}_f^{\,2}(t). \end{aligned} \tag{7}$$

The velocity $\vec{v}_f$ is the instantaneous velocity of the body, when described in an inertial frame of referenc. At the section $\partial\Omega_2$ outflow boundary conditions are assumed. Along $\partial\Omega_3$ in front of the

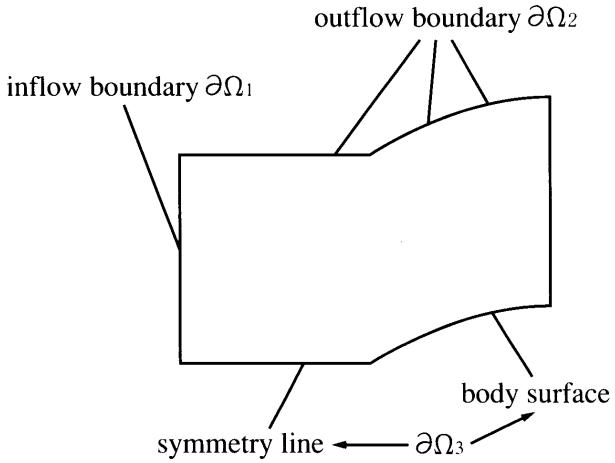

Fig. 1: Flow region

body a symmetry condition is fulfilled, and on the body contour which may be curved or a straight line we impose for the Eulerian equations the condition

$$\vec{v} \cdot \vec{n} = 0, \tag{8}$$

$$\vec{v}_{body} = \vec{0}, \tag{9}$$

where $\vec{n}$ denotes the local normal unit vector on the body surface. In addition an adiabatic behavior of the flow field is assumed on the body surface. E is the specific total energy. Further boundary conditions are imposed on ρ and E:

$$\nabla\rho \cdot \vec{n} = 0 \text{ ; and } \nabla E \cdot \vec{n} = 0. \tag{10}$$

3. THE ALGORITHM FOR THE EULERIAN APPROACH

For the numerical simulation of the time-dependent flow around wedges or cones, a body fitted coordinate system is used. In the physical plane the region close to the body nose is spatially resolved by a fine grid, and also in the neighborhood of the body surface the grid lines are attracted. Several grids were used for the calculations to show that the results are independent of the chosen grid distribution.

The basic system of equations is written in conservative variables as follows:

$$(\vec{U})_t+(\vec{F}(\vec{U}))_x+(\vec{G}(\vec{U}))_y+\delta\vec{B}(\vec{U})=\vec{A}(\vec{U}). \tag{11}$$

δ denotes the values 0 or 1 according to the plane or axisymmetrical geometry under consideration, respectively. The vector functions $\vec{U}$,$\vec{F}$,$\vec{G}$,$\vec{B}$, and $\vec{A}$ are defined in the following way:

$$\vec{U}=\begin{pmatrix}\rho\\ \rho u\\ \rho v\\ E\end{pmatrix}, \tag{12}$$

$$\vec{F}(\vec{U})=\begin{pmatrix}\rho u\\ \rho u^2+(\gamma-1)\left[E-\frac{1}{2}\rho(u^2+v^2)\right]\\ \rho uv\\ u\left[\gamma E-(\gamma-1)\frac{1}{2}\rho(u^2+v^2)\right]\end{pmatrix}, \tag{13}$$

$$\vec{G}(\vec{U})=\begin{pmatrix}\rho v\\ \rho vu\\ \rho v^2+(\gamma-1)\left[E-\frac{1}{2}\rho(u^2+v^2)\right]\\ v\left[\gamma E-(\gamma-1)\frac{1}{2}\rho(u^2+v^2)\right]\end{pmatrix}, \tag{14}$$

$$\vec{A}(\vec{U})=\begin{pmatrix}0\\ -\rho a_x\\ -\rho a_y\\ (-\rho\vec{a})\vec{v}\end{pmatrix}, \qquad \vec{B}(\vec{U})=\frac{1}{y}\begin{pmatrix}\rho v\\ \rho vu\\ \rho v^2\\ v\left[\gamma E-(\gamma-1)\frac{1}{2}\rho(u^2+v^2)\right]\end{pmatrix}. \tag{15}$$

The numerical fluxes are modelled by an approximate solution of the Riemann-problem. The flow variables are assumed to be constant in each cell. At the cell boundary the flux is calculated by the values of the left and right neighbor cell. This leads by extrapolation with a weighting factor κ to the following formulas:

$$\bar{U}^{n(L)}_{i+\frac{1}{2}} = \bar{U}^{n}_{i}+\frac{1}{4}\left[(1-k)(\bar{U}^{n}_{i}-\bar{U}^{n}_{i-1})+(1+k)(\bar{U}^{n}_{i+1}-\bar{U}^{n}_{i})\right], \tag{16}$$

$$\bar{U}^{n(R)}_{i+\frac{1}{2}} = \bar{U}^{n}_{i}-\frac{1}{4}\left[(1+k)(\bar{U}^{n}_{i+1}-\bar{U}^{n}_{i})+(1-k)(\bar{U}^{n}_{i+2}-\bar{U}^{n}_{i+1})\right]. \tag{17}$$

This is used for an approximation of the numerical fluxes of second order accuracy. The time integration is performed by a splitting into two half steps to gain second order accuracy. The whole algorithm is split for the two-dimensional problem which leads to the following sequence of operations

$$\bar{U}^{n+1}=\mathcal{L}_\xi\left(\frac{\Delta t}{2}\right)\mathcal{L}_\eta(\Delta t)\;\mathcal{L}_\xi\left(\frac{\Delta t}{2}\right)\bar{U}^{n}. \tag{18}$$

4. RESULTS OF EULERIAN EQUATIONS AND DISCUSSION

The main problem for the comparison of numerical data with analytical formulas due to Cabannes is the identification of the shock front. In the present investigation the curvature of the shock wave is determined by the least square method. The points on the shock wave are calculated by a polynomial ansatz of second degree. In Fig. 2 the approximation of a shock wave is shown. The variation of the radii of curvature for an accelerated and also for a decelerated wedge is given in the Fig. 3. The two curves show the radii of curvature for several Mach numbers. Starting with the initial condition at t=0 for the flow field variables at Mach number M=1.8 the radii of curvature are calculated for different times when the Mach number changes due to the acceleration of the wedge. Therefore, the Mach number variation corresponds to the increase of time for which the numerical simulations were carried out. For a decelerated wedge the starting Mach number was chosen to be M=2.5, and the radii of curvature are plotted in Fig. 3 down to the Mach number of M=1.7.

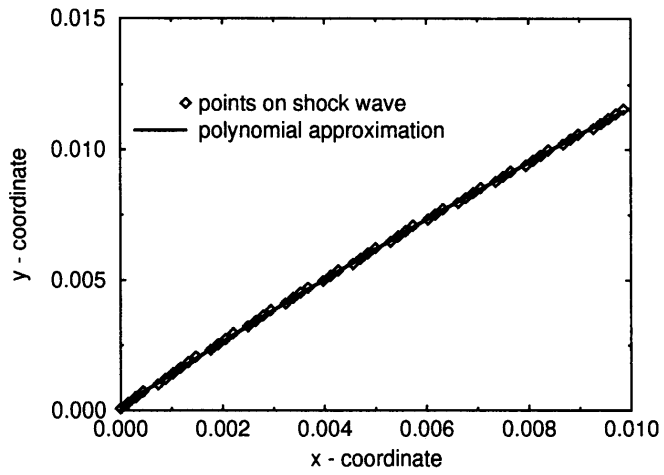

Fig. 2: Polynomial approximation of the shock wave contour

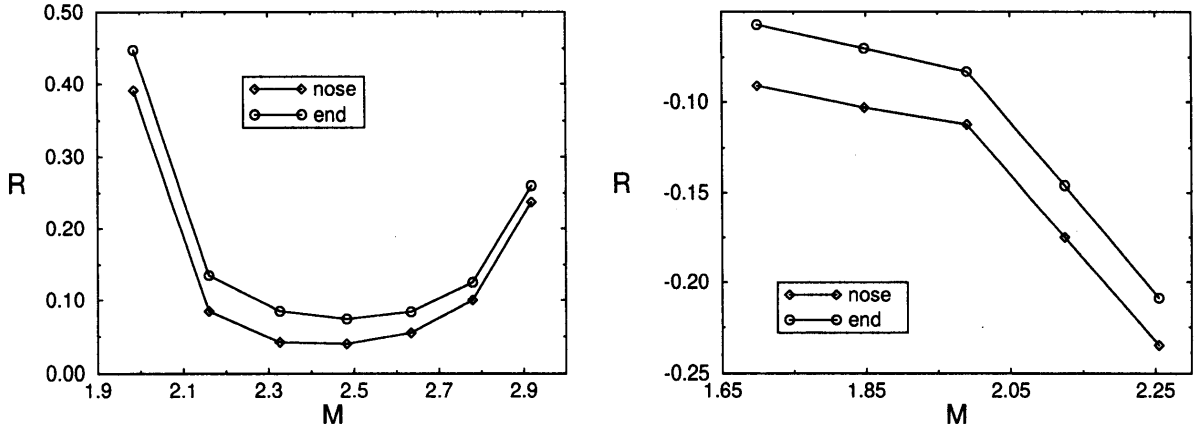

Fig. 3: Radii of curvature of the shock wave for an accelerated wedge (left) and a decelerated one (right)(θ s=15°)

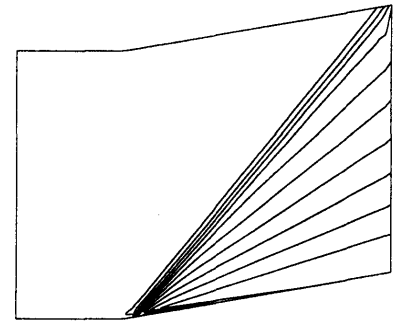

$t = 0.000\text{e-}2,\ M = 1.3$

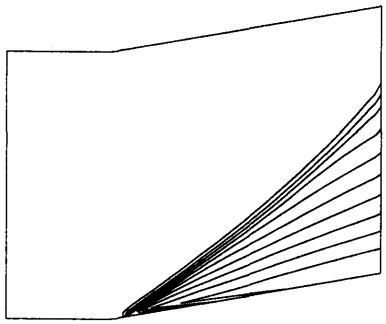

$t = 1.484\text{e-}2,\ M = 1.782$

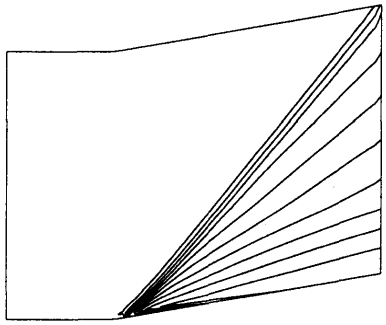

$t = 0.399\text{e-}2,\ M = 1.430$

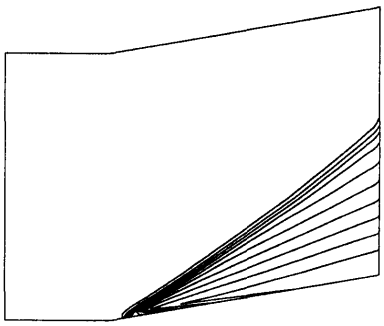

$t = 1.816\text{e-}2,\ M = 1.890$

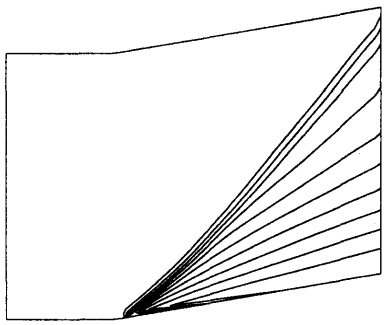

$t = 0.771\text{e-}2,\ M = 1.553$

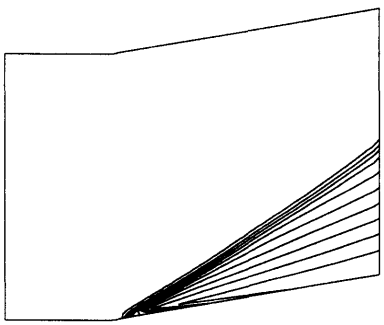

$t = 2.137\text{e-}2,\ M = 1.994$

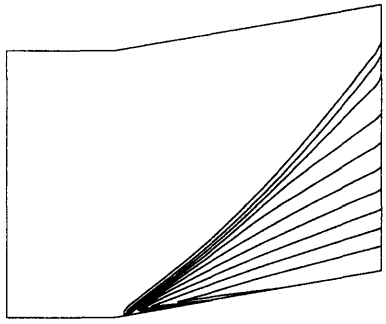

$t = 1.138\text{e-}2,\ M = 1.670$

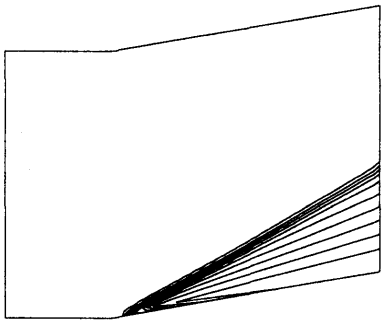

$t = 2.746\text{e-}2,\ M = 2.193$

Fig. 4:Isopycnic curves of the flow field around an accelerated cone (θ s=10°, a=25) for different time steps

As an example of the time-dependent flow around a cone with an aperture angle of 20° in Fig.4 the time sequence is shown for the evolution of the flow field for the acceleration a=25. The Mach number varies from the initial value M=1.3 to its final value M=2.193. This plot of the isopycnic curves demonstrates the change of the curvature of the shock wave during a time interval of $\Delta t=0.02746$. A comparison of the asymptotic results due to Cabannes with the numerical data is shown in Fig.5. The calculations were started from a flow field around a wedge at Mach number M=2.5. At the nose and at the end of the finite body the radii of the curvature are plotted. For the decelerated wedge (a=-20) with the aperture angle of 30° a good agreement is seen for the Mach number interval

$$1.9<M<2.25.$$

It has to be taken into account, that a finite length of the body will naturally influence the flow field around the nose of a body, as experiments and numerical investigations have shown. Under the expansion wave which is present at the rear part of a wedge or cone with finite length the shape of the whole shock wave will be influenced. Insofar the numerical results are valid only for very long bodies in unsteady supersonic flows.

The calculations according to the Eulerian equations for the wedge geometry and the comparison with Cabannes' results were performed by S. Kasten [6] on the basis of a computer code which was developed by Chr. Hartmann [7].

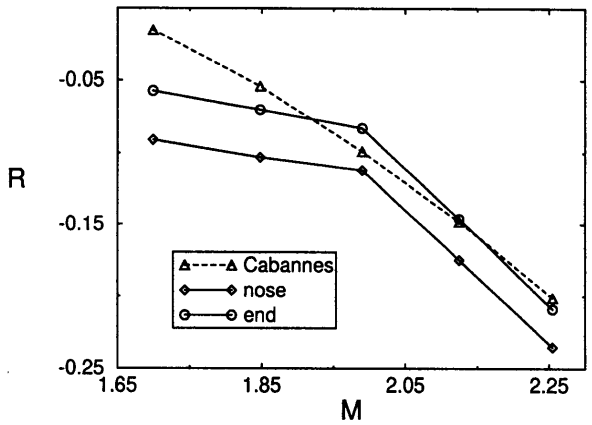

Fig. 5:Comparison of the analytical and numerical radii of curvature for a decelerated wedge (θ s=15°, a=-20)

5. COMPARISON WITH RESULTS FROM COMPRESSIBLE NAVIER-STOKES EQUATIONS

All numerical simulations for the Eulerian and the Navier-Stokes equations were started from a stationary flow field at a given Mach number (Fig.6). In the following the results for the flow around a wedge of 10°half opening angle are summarized, and starting with the Mach number 2, the same number of time steps were followed in the evolution of the flow field, once for the nonviscous flow and then for the viscous flow for a Reynolds number of 50000. The Reynolds number was defined according to:

$$Re = \frac{Lc_\infty}{v_\infty}. \tag{19}$$

The typical length scale L is given by the length of the ramp of the wedge,c_∞ and V_∞ are the speed of sound and the kinematic viscosity at infinity.

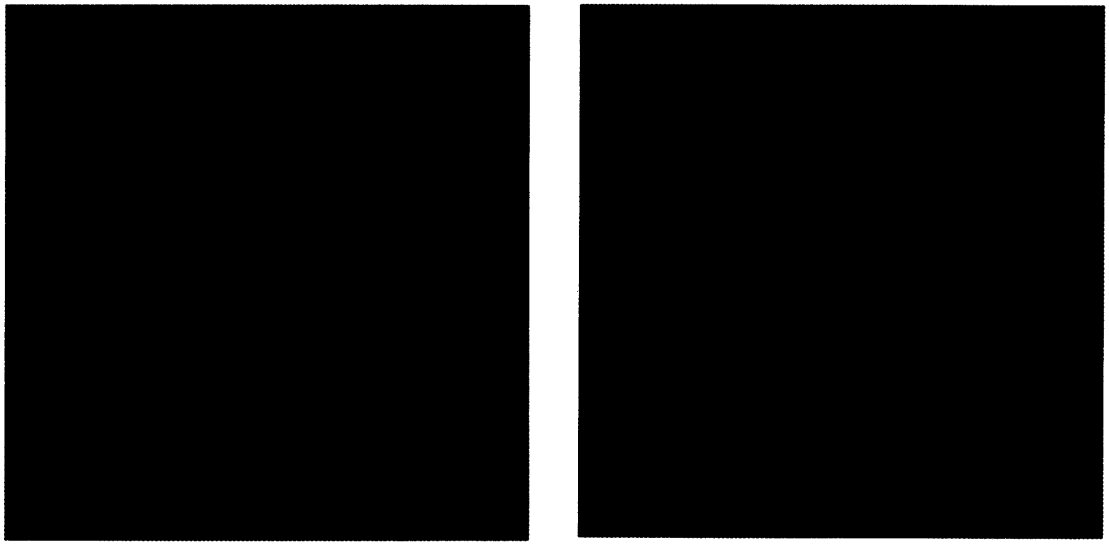

Fig. 6: Stationary solution for the flow around a wedge of half opening angle of 10°at Mach number Ma=2. Left: Euler, right: Navier-Stokes (Density field)

It can be seen from Fig.6 that for the stationary flow field the attached shock waves of the Navier-Stokes calculation shows a much stronger curvature at the tip of the wedge than the straight shock, calculated for the Eulerian equations.

If the evolution of the flow field and the shock is followed for both the cases (Euler and Navier-Stokes) up to the time

$$t = 3.68 \times 10^{-2}, \tag{20}$$

which corresponds to a dimensionless acceleration of a=20, and a Mach naumber of the oncoming gas stream of

$$M = 3.47, \tag{21}$$

the shock in nonviscous flow already starts to get a slightly concave shape (Fig.7) while the shock front of the Navier-Stokes solution still remains convex, looking from the upstream direction.
This behavior of the two solutions from the nonviscous and the viscous flow calculations is typical for even later times of the evolution. In Fig.8 the two flow fields are compared for the time step

$$t = 6.43 \times 10^{-2}, \tag{22}$$

and a corresponding Mach number

$$M = 4.57 . \tag{23}$$

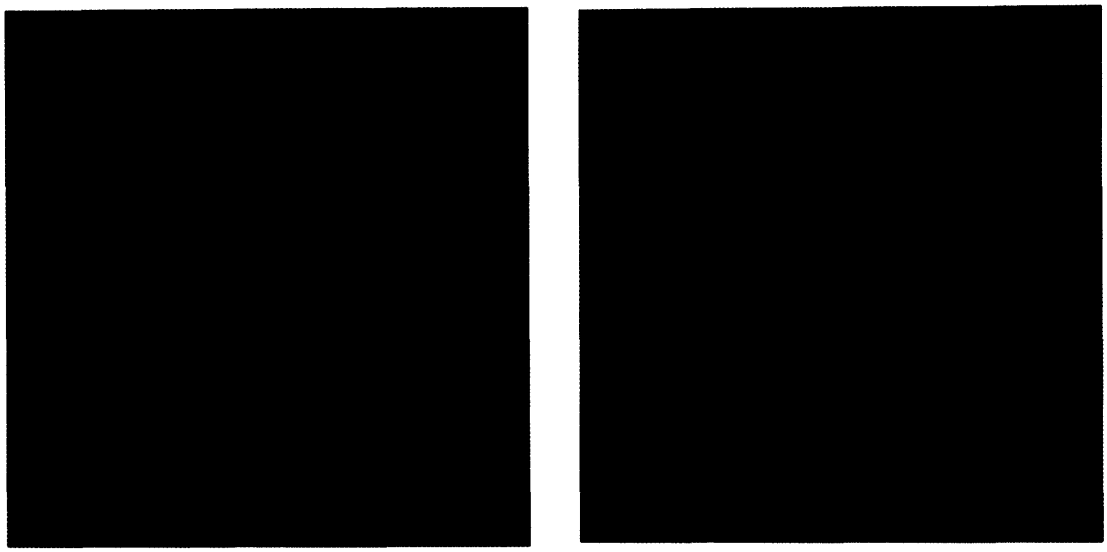

Fig. 7: Attached shock wave at the wedge with half opening angle of 10° in a flow with constant acceleration of a=20 at time $t = 3.68 \times 10^{-2}$,(M=3.47). Left: Euler, right: Navier-Stokes (Density field)

It is evident that the shock approaches more and more the body surface, but the region between shock wave and wedge is for the Navier-Stokes solution much larger than for the Eulerian solution. The viscosity effects lead naturally to a boundary layer along the wedge which thickens the region between body and shock. Therefore, a comparison of the two flow fields should take into account the boundary layer thickness for the viscous flow in order to correct the half opening angle of the wedge for the nonviscous flow.

It seems to be evident that a realistic shock wave simulation has to be based on the compressible Navier-Stokes equations. This would also have a strong influence on the calculation of the curvature of the attached shock at the tip of the body.

Fig. 8: Accelerated supersonic flow over a wedge of half opening angle of 10° at time $t=6.43\times10^{-2}$,(M=4.57). Left: Euler,right: Navier-Stokes (Density field)

For the same geometry the evolution of the density field is calculated for a later time. In Fig.9 the shock front is represented for the time t=0.11 and the corresponding Mach number M=6.27.

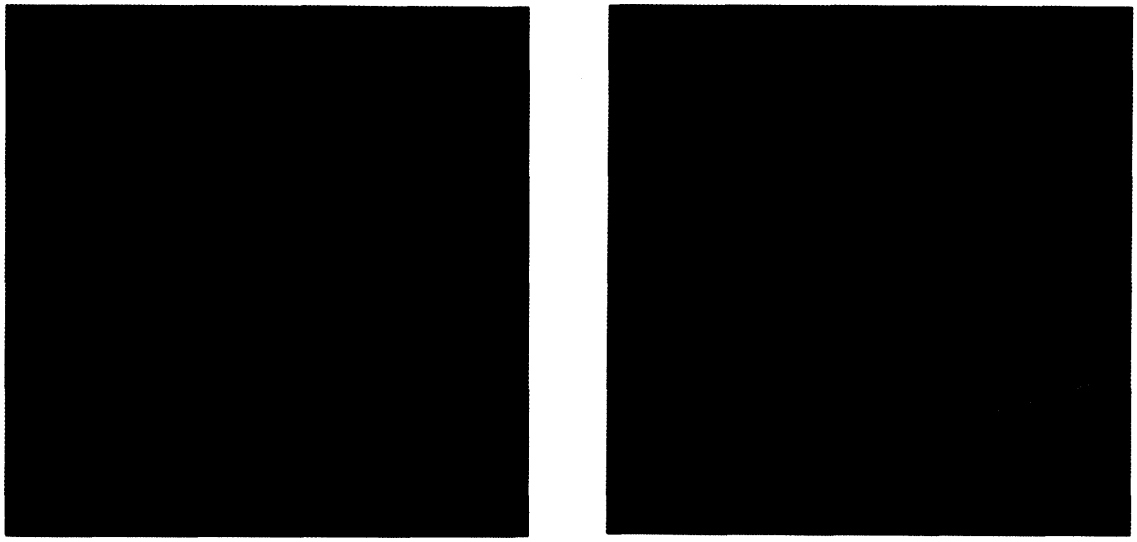

Fig. 9: Shock front an time t = 0.11. M= 6.27. Left: Euler,right: Navier-Stokes (Density field)

In the last Fig.10 the stationary flow at Mach number M=2 around a parabolic profile is shown, performed on the basis of the compressible Navier-Stokes equations for a Reynolds number

$$Re=5\times10^{4}.$$

The tangent at the tip of the contour has an inclination of 20°and at the end of the body of 5°. The density plot shows a strong compression at the nose.

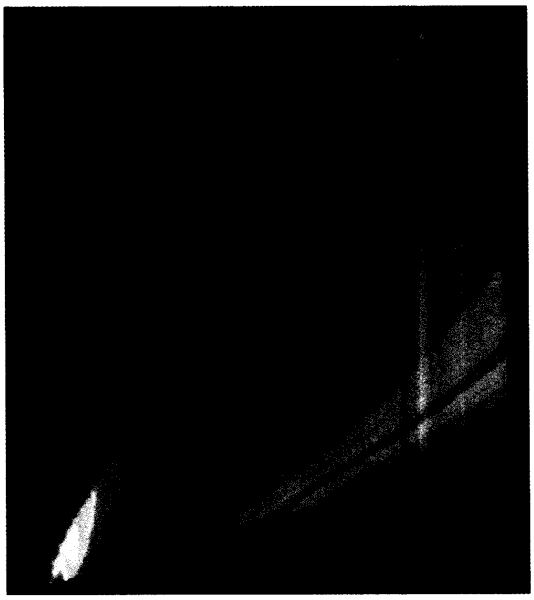

Fig. 10: Attached shock wave for a parabolic profile at Mach number M=2 for the stationary viscous flow at Reynolds number Re=50000

6. CONCLUSION

The supersonic Mach number flows for accelerated and decelerated bodies of wedge-like or conical shape were simulated numerically on the basis of the Eulerian and the compressible Navier-Stokes equations. A comparison with analytical investigations by Cabannes [3] shows a good agreement for e.g. the radii of curvature for a decelerated wedge (Fig.5). The slight discrepancy at low Mach numbers around 1.65 is probably due to the low order of the analytical approximation in Cabannes' results.

The main difference between the results based on the Eulerian and the Navier-Stokes equations is seen in Fig.7, where the curvature of the shock wave at the nose of the wedge is influenced by the different boundary conditions on the body surface. The boundary layer in the viscous flow regime thickens the effective body surface and acts significantly on the shape of the attached shock wave. Therefore a reliable calculation of the curvatures of accelerated or decelerated shock waves is only possible by taking into account the viscosity and compressibility of the gas, in order to get an agreement with experimental results.

References

[1] Cabannes, H. Etude de l' onde de choc atachée dans les écoulements de révolution, La Rech. Aéro. no. 24, (1951), 17-23

[2] Cabannes, H. Etude de l' onde de choc atachée dans les écoulements de révolution, La Rech. Aéro. no. 27, (1952), 7-16

[3] Cabannes, H.: Influence des accélérations sur la courbure des chocs, La Rech. Aéro., no. 39,(1954), 2-13

[4] Whitham, G.B. The Flow Pattern of a Supersonic Projectile, Comm. Pure and Appl. Math., Vol.5,(1952), 301-348

[5] Rao, P.S. Supersonic Bangs, Part I and II, Aeron. Quart., 7, (1956), 135-155

[6] Kasten, S. Ueber den Zusammenhang von Körpergeometrie und Stoβstruktur von instationaer angestroemten Koerpern im Überschall, Diplomarbeit-Darmstadt, 1997

[7] Hartmann, Chr. Numerische Simulation dreidimensionaler Stoβfokussierungseffekte, Dissertation-Darmstadt, 1996